Water Research 173 (2020) 115551

Contents lists available at ScienceDirect

Water Research

journal homepage: www.elsevier.com/locate/watres

Evaluating the effects of water matrix constituents on micropollutant removal by activated carbon and β-cyclodextrin polymer adsorbents

Yuhan Ling [a], Diego M. Alzate-Sánchez [b], Max J. Klemes [b], William R. Dichtel [b, **], Damian E. Helbling [a, *]

[a] School of Civil and Environmental Engineering, Cornell University, Ithaca, NY, 14853, USA
[b] Department of Chemistry, Northwestern University, Evanston, IL, 60208, USA

ARTICLE INFO

Article history:
Received 19 October 2019
Received in revised form
18 January 2020
Accepted 25 January 2020
Available online 27 January 2020

Keywords:
Micropollutant
Adsorption
Breakthrough
Fouling
Activated carbon
β-cyclodextrin polymer

ABSTRACT

The performance of adsorbents for the removal of organic micropollutants (MPs) from water can be influenced by the presence of water matrix constituents. The objective of this research was to evaluate the influence of water matrix constituents on the performance of coconut-shell activated carbon (CCAC), porous β-cyclodextrin polymer (CDP), and CDP coated on cellulose microcrystal (CDP@CMC) adsorbents. MP removals were measured in batch experiments for a mixture of 90 MP at 1 μg L^{-1} and MP breakthrough was measured in rapid small-scale column test (RSSCT) experiments for a mixture of 15 MP at 500 ng L^{-1}. All experiments were performed first with nanopure water, and subsequently with six different water samples collected from two separate groundwater, surface water, and wastewater effluent sources. The results of batch and RSSCT experiments demonstrate more rapid adsorption kinetics and less adsorption inhibition in the presence of matrix constituents for CDP adsorbents relative to CCAC. Further, the treatment capacity of CDP@CMC in the RSSCT experiments was higher than that of CCAC, particularly in more complex water matrices. Statistical analyses were performed to investigate associations between adsorption inhibition among groups of MPs and the concentrations of specific water matrix constituents. For CCAC, adsorption inhibition was observed for all MPs and was primarily attributed to the presence of dissolved organic matter with molar weight less than 1000 Da. For CDP adsorbents, adsorption inhibition was primarily observed for cationic MPs and was attributed to the screening of the negative surface charge of CDP by inorganic ions in water samples with high ionic strength. These data further demonstrate the value of CDP as an alternative adsorbent to CCAC for the removal of MPs during water and wastewater treatment.

1. Introduction

Natural water resources have been contaminated by a variety of anthropogenic organic chemicals, of which some are referred to as micropollutants (MPs) due to their typical occurrence at trace levels in the environment (Carpenter and Helbling, 2018; Carpenter et al., 2019; Schwarzenbach et al., 2006). Because of their diverse physicochemical properties and low concentrations, MP removal is generally limited in conventional water and wastewater treatment processes (Benner et al., 2013). Activated carbon (AC) adsorption has emerged as a leading technology and has been demonstrated to effectively remove a broad spectrum of MPs (Bonvin et al., 2015; Kennedy et al., 2015; Margot et al., 2013). However, limitations of AC adsorption arise from relatively slow kinetics (Bonvin et al., 2015), poor removal of polar MPs (Kovalova et al., 2013), and fouling by dissolved organic matter (DOM) and other matrix constituents (Kennedy and Summers, 2015; Zietzschmann et al., 2016). Further, the expenses of applying AC in water and wastewater treatment processes are generally high because of the significant energy required for AC regeneration (Margot et al., 2013). To

Abbreviations: AC, activated carbon; BA-UF, batch adsorption followed by ultrafiltration; CCAC, coconut-shell activated carbon; CDP, β-cyclodextrin polymer; CDP@CMC, β-cyclodextrin polymer grafted on cellulose microcrystals; DOM, dissolved organic matter; HPLC-MS/MS, high performance liquid chromatography and tandem mass spectrometry; MP, micropollutant; MW, molar weight; PBF, packed bed filtration; QSAR, Quantitative Structure-Activity Relationship; RSSCT, Rapid Small-Scale Column Test; SD, Supplementary Data.

* Corresponding author.
** Corresponding author.
E-mail addresses: wdichtel@northwestern.edu (W.R. Dichtel), damian.helbling@cornell.edu (D.E. Helbling).

https://doi.org/10.1016/j.watres.2020.115551
0043-1354/

address these deficiencies, alternative adsorbents such as porous β-cyclodextrin polymers (CDPs) (Alsbaiee et al., 2015; Ling et al., 2017) have been developed for potential implementation in batch adsorption followed by ultrafiltration (BA-UF) processes. More recently, CDPs coated on cellulose microcrystals (CDP@CMC) have been developed by polymerizing CDPs in the presence of CMCs, resulting in adsorbents with larger particle sizes amenable for packed bed filtration (PBF) processes (Alzate-Sánchez et al., 2019).

The fouling of AC by water matrix constituents is perhaps the major concern for MP removal in both BA-UF and PBF processes (Bonvin et al., 2015; Zietzschmann et al., 2016). MPs adsorb to AC materials primarily by means of hydrophobic interactions, though charged functional groups on AC surfaces can also facilitate the adsorption of ionic MPs by means of electrostatic interactions (Ling et al., 2019). As AC adsorption is non-selective, both MPs and DOM, which is generally present in all waters from either natural or anthropogenic sources, can be adsorbed by means of hydrophobic and electrostatic interactions. According to previous research, the adsorption of MPs on AC can be inhibited through direct site competition with low and medium molecular weight (MW) DOM that is similar in size and charge state to MPs and through pore blockage caused by high MW DOM (Ding et al., 2008; Li et al., 2003; Newcombe et al., 1997). In addition, the presence of inorganic ions in the bulk water can diminish the surface charge of AC by screening local ionizable functional groups, thereby limiting their electrostatic interactions with MPs (Newcombe and Drikas, 1997; Summers and Roberts, 1988). For example, the coconut shell AC (CCAC) employed in this study exhibits a positive surface charge at neutral pH (de Ridder et al., 2013). Therefore, the adsorption of anionic MPs on CCAC could be inhibited by negatively charged, low MW DOM through direct site competition and/or by the presence of inorganic anions that screen the positive surface charge (Newcombe and Drikas, 1997; Summers and Roberts, 1988). Though the mechanisms of adsorption inhibition on AC adsorbents have been evaluated in previous research, how adsorbent fouling will influence the removal of diverse groups of MPs in BA-UF and PBF processes remains less clear because previous studies were either performed with very limited types of MPs (e.g., neutral MPs) or with high concentrations of MPs that were not environmentally relevant (Bonvin et al., 2015; Kennedy and Summers, 2015; Sgroi et al., 2018; Zietzschmann et al., 2016).

In our previous study, a tetrafluoroterephthalonitrile (TFN) crosslinked CDP exhibited rapid adsorption kinetics and efficient removal of a variety of MPs, and was not fouled by humic acid (a surrogate for DOM) or sodium chloride (a surrogate for inorganic ions), demonstrating its potential as an alternative adsorbent to AC for MP removal during water and wastewater treatment (Ling et al., 2017). MP adsorption on CDP relies on the formation of host-guest complexes in the 0.78 nm interior cavity of the β-cyclodextrin monomer, which requires adsorbates to fit within a certain size range (Ling et al., 2019, 2017). Additionally, CDP exhibits a negative surface charge at neutral pH (Klemes et al., 2018). The specific role that the negative surface charge of CDP plays in MP adsorption is unknown, though enhanced adsorption affinity for cationic MPs has been observed (Ling et al., 2017). While CDP is not fouled by humic acid and NaCl, we could expect that smaller DOM molecules could inhibit MP uptake through direct-site competition by binding in the interior cavity of the β-cyclodextrin monomer. Further, positively charged DOM and the presence of inorganic cations could screen the negative surface charge of CDP, thereby lowering the adsorption affinity for cationic MPs.

To further our understanding of the fouling of CCAC and CDP by natural matrix constituents, we designed experiments to explore the removal of MPs by means of CCAC and CDP adsorption in environmentally derived water samples with varying types and amounts of DOM and inorganic ions. The objectives of the research were to: (1) benchmark the performance of CCAC and CDP in simulated BA-UF processes with water samples from six different sources with 90 MPs; (2) benchmark the performance of CCAC and CDP@CMC in rapid small-scale column test (RSSCT) experiments that simulate PBF processes with water samples from different sources with 15 MPs; and (3) identify the water matrix constituents contributing most to adsorption inhibition on CCAC, CDP, and CDP@CMC. Our results demonstrate less adsorption inhibition and greater treatment capacity for CDP adsorbents relative to CCAC. We also identified specific water matrix constituents that are associated with the adsorption inhibition of certain groups of MPs. These data significantly improve our understanding of the mechanisms by which CCAC and CDP adsorbents remove MPs from water, and support the continued evaluation of CDPs as alternative adsorbents for use in BA-UF or PBF processes during water and wastewater treatment.

2. Materials and methods

2.1. Chemicals and adsorbents

All experiments with nanopure water were performed at pH 6.7; the pH was confirmed to be stable by measuring pH throughout each experiment. All experiments with real water samples were performed at the original pH of the water samples without adjustment. We selected 90 and 15 MPs for batch and RSSCT experiments, respectively, according to their environmental relevance (Bradley et al., 2017; Carpenter and Helbling, 2018; Pochodylo and Helbling, 2017), their broad range of physiochemical properties, and previous studies exploring their adsorption on CCAC and CDP (Ling et al., 2019, 2017; Rossner et al., 2009). A list of all MPs along with their measured LogK_D values for CCAC and CDP and charge state at neutral pH is provided in Table S1 of the Supplementary Data (SD); all LogK_D values were measured experimentally in a previous study for each MP-adsorbent pair (Ling et al., 2019). We selected 44 isotope-labeled internal standards (ILISs) to account for the matrix effects of different water samples on the quantification of MPs. A list of all ILISs along with their suppliers is provided in Table S2 of the SD. The preparation of stock solutions for each MP and two analytical mixtures containing the 90 and 15 MPs were performed as previously described (Li et al., 2018). For batch experiments, CCAC and CDP adsorbents were prepared and synthesized according to previously established methods (Alsbaiee et al., 2015; Ling et al., 2017). Briefly, the CCAC is commercially available (AquaCarb 1230C, Westates Carbon, Siemens, Roseville, MN) and has an average particle size of 850 μm; the as-synthesized CDP has an average particle size on the order of 50−60 μm. To increase the similarity in particle size between the CCAC and CDP, the CCAC was pulverized with a mortar and pestle until >95% (mass) passed a 74-μm sieve (200 U.S. mesh). For RSSCT experiments, the CCAC was pulverized with a mortar and pestle to achieve an average particle diameter of approximately 125 μm with 100 × 200 U.S. standard mesh (Kennedy and Summers, 2015). The CDP@CMC, with an average particle diameter of approximately 125 μm, was synthesized according to a previously published method (Alzate-Sánchez et al., 2019). The particle size, surface area, and porosity for these adsorbents were previously reported and are provided in Table S3 (Alsbaiee et al., 2015; Alzate-Sánchez et al., 2019; Ling et al., 2017).

2.2. Water samples

Six water samples collected from two separate groundwater (GW1 and GW2), surface water (SW1 and SW2), and wastewater effluent sources (WW1 and WW2) were employed in this study. All experiments were also performed in nanopure water, against

which the performance of the adsorbents in environmentally derived water samples were benchmarked. Each water sample was characterized for its pH, dissolved organic carbon (DOC, a surrogate measurement for DOM) concentration, total dissolved solids (TDS) concentration, conductivity, and inorganic ion concentrations using standard methods (Baird et al., 2017). Further, to investigate the effect of DOM size on MP adsorption, we characterized the MW distribution of DOM in each water sample through high-performance, size-exclusion chromatography (HPSEC) followed by total organic carbon (TOC) analysis; more details are provided in the SD (including a description of our procedure and an example chromatogram provided in Fig. S1). All water samples were pre-filtered with a 47 mm GF/F glass-fiber membrane (Whatman) and a 0.45 μm polyethersulfone syringe filter successively to remove suspended solids before they were employed in adsorption experiments (Knappe et al., 1997; Zietzschmann et al., 2016).

2.3. Batch experiments

Batch experiments to evaluate the fouling of CCAC and CDP in BA-UF processes were performed in 100 mL of water in 125 mL glass Erlenmeyer flasks with magnetic stir bars on a multi-position stirrer (VWR) with a stirring rate of 400 revolutions per minute (rpm) at 23 °C. MPs were spiked to generate an additional concentration of each adsorbate of 1 μg L^{-1} to any background concentration of the MPs that may have been present. Experiments investigating CCAC and CDP were both performed at an adsorbent dose of 10 mg L^{-1}. These adsorbate and adsorbent doses were selected according to previous research investigating MP removal by CCAC and CDP adsorbents (Ling et al., 2019, 2017), and previous research regarding the application of AC in BA-UF processes (Bonvin et al., 2015). The restoration of the dried adsorbents was performed as previously described to create a suspension of each adsorbent (Ling et al., 2017). Briefly, 10 mg of adsorbent was added to a 20 mL amber vial containing nanopure water (10 mL) to yield a 1 g/L suspension. The suspension was mixed with a vortex mixer (Fisher Scientific) for 30 s, sonicated for 1 min to break small aggregates, and then stirred on a multiposition stirrer for 30 min at 360 rpm. Following this restoration procedure, appropriate volumes of water samples, the analytical MP mixture (90 MPs, each MP at 100 μg L^{-1}), and the adsorbent suspension (1 g/L) were added to each flask successively. Samples were collected in 8 mL volumes after 1 h of contact time and filtered through a 0.22 μm PVDF syringe filter (Restek). This contact time was selected according to previous research exploring MP removal by CCAC and CDP adsorbents and typical hydraulic retention times in BA-UF processes (Bonvin et al., 2015; Ling et al., 2019, 2017). Control experiments to account for other MP losses were performed under the same conditions with no addition of adsorbent. All experiments were performed in triplicate. The samples were analyzed by means of high-performance liquid chromatography and tandem mass spectrometry (HPLC-MS/MS) to determine the concentration of each MP in the aqueous phase. The removal efficiency of each MP was determined by the following equation:

$$R_{MP} = \frac{C_0 - C_t}{C_0} \times 100 \qquad \text{Equation 1}$$

where R_{MP} is the percent removal of each MP; C_0 (ng L^{-1}) is the average concentration of a MP in the samples of the control experiments; C_t (ng L^{-1}) is the concentration of a MP in the liquid phase at sampling time t. We defined a fouling scale index (FSI) as a metric to quantify the extent of adsorption inhibition for each MP in each experiment relative to the adsorption in nanopure water. The FSI for batch experiments was determined by the following equation:

$$\textit{Fouling Scale Index} = \frac{\sum(R_{MP}\ \textit{in NP} - R_{MP}\ \textit{in a water sample})}{\sum R_{MP}\ \textit{in NP}} \times 100 \qquad \text{Equation 2}$$

2.4. RSSCT experiments

For the RSSCT experiments with CCAC and CDP@CMC, a stainless-steel HPLC column (Restek) with an inside diameter of 0.4 cm, a column length of 3 cm, and stainless-steel frits was employed as the host of packed-bed adsorption materials. A Shimadzu LC-20AD pump with parallel double micro plunger was employed to deliver a constant flow rate of 1 mL min^{-1} of feed solution for all RSSCT experiments. All RSSCT experiments were performed with a simulated empty bed contact time (EBCT) of 9.6 min. The CCAC and CDP@CMC tested in the column experiments both had an average particle size of 125 μm. The flow rates, particle sizes, and the dimensions of the RSSCT column were determined according to the constant diffusivity approach (Crittenden et al., 1991, 1986), which has been successfully applied in previous research to simulate pilot-scale MP breakthrough (Knappe et al., 1997). Detailed information on the RSSCT experiments and the simulated column can be found in Table S4 of the SD. We note that RSSCT experiments were selected as a test system to compare the performance of CCAC and CDP@CMC under uniform experimental conditions, similar to a previous study employing RSSCT to evaluate the potential of ion exchange resins for the removal of perfluoroalkyl acids (Schaefer et al., 2019); robust extrapolation of the results from the RSSCT experiments to the simulated system would require further validation, particularly for the CDP@CMC adsorbent.

All natural water samples were pre-filtered with a 47 mm GF/F glass-fiber membrane (Whatman) and a 0.45 μm polyethersulfone syringe filter to remove suspended solids. Then, the analytical MP mixture (15 MPs, each MP at 100 μg L^{-1}) was spiked into each water sample to generate an additional concentration of each MP at 500 ng L^{-1} to any background concentration of the MPs that may have been present. Though the designed dimensions of the RSSCT columns for both materials are identical, due to their different densities, the mass of CCAC and CDP@CMC packed into the columns to achieve a 1 cm bed depth are ~85 mg and ~65 mg per column, respectively. The RSSCT columns were run continuously until all 15 MPs exhibited over 10% breakthrough or the predetermined 60,000 bed volumes of treatment were achieved; we selected 60,000 bed volumes of treatment as a conservative threshold for the economical usage of CCAC or CDP@CMC for drinking water production, which is often cited as 15,000 bed volumes of treatment (Kennedy et al., 2015). Samples were collected in 8 mL volumes on an hourly basis and filtered through a 0.22 μm PVDF syringe filter before they were analyzed by means of HPLC-MS/MS. To confirm that influent concentrations of all MPs remained constant throughout each RSSCT experiment, samples were collected at the influent of the column every 24 h for each test. These samples were also filtered and analyzed by means of the same method. The adsorbent use rate of CCAC and CDP@CMC for each MP was determined by the following equation:

$$\textit{Adsorbent Use Rate} = \frac{\rho_{adsorbent}}{BV_{10\%}} \qquad \text{Equation 3}$$

where $BV_{10\%}$ is the 10% breakthrough bed volumes of each MP on each adsorbent in each water matrix and $\rho_{adsorbent}$ is the density of

each adsorbent (mg L^{-1}).

The FSI for RSSCT experiments was determined by the following equation:

$$Fouling\ Scale\ Index = \frac{\sum(BV_{10\%}\ in\ NP - BV_{10\%}\ in\ a\ water\ sample)}{\sum BV_{10\%}\ in\ NP} \times 100$$

Equation 4

We selected $BV_{10\%}$ as the metric to evaluate adsorption inhibition based on previous research (Kennedy and Summers, 2015; Zietzschmann et al., 2016).

2.5. Analytical methods

The quantification of analytes in samples from the batch experiments and RSSCT experiments was performed by means of HPLC-MS/MS (QExactive, ThermoFisher Scientific). The analytical method is described in the SD and analytical details used for the detection and quantification of each analyte can be found in Table S5 of the SD.

3. Results and discussion

3.1. Water characterization

The six environmentally derived water samples were selected for their diverse matrix compositions and their relevance for water and wastewater treatment. Each water sample was characterized for general water quality parameters including pH, DOC concentration (a surrogate measurement for DOM), conductivity, TDS concentration, and the concentrations of several target inorganic ions. All water characterization data are provided in Table 1.

The pH of the six water samples were all between 8.1 and 8.3, which is consistent with pH measurements of water samples from the same region reported in previous research (Carpenter et al., 2019). Due to the minor pH differences among these water samples, no further insights can be achieved into the impacts of pH on MP removal by CCAC and CDP adsorbents in these water samples. However, it is worth noting that MP removal by CDP can be enhanced at pH values lower than 5 (Li et al., 2018). The conductivity and TDS measurements generally demonstrate increasing ionic strength from the relatively clean groundwater matrices to the more complex surface water and wastewater effluent matrices. The concentrations of several target inorganic ions also demonstrate an expected increase from groundwater to wastewater, with a couple of notable exceptions; the nitrate (NO_3^-) concentration was highest in GW2 and sulfate (SO_4^{2-}), magnesium (Mg^{2+}), and calcium (Ca^{2+}) concentrations were more uniform across the water samples.

The remaining data in Table 1 provide the characterization results of the DOM MW distributions for each water sample. The concentrations of DOM (i.e., unfractionated water samples) in all water samples fit well into the respective typical ranges of DOM in groundwater, surface water, and wastewater effluent (Sgroi et al., 2018; Thurman et al., 1982; Wagoner et al., 1997) with one exception; the DOM concentration in SW2 was anomalously high. We note that the water collected from this site was rather turbid and contained some algae and other planktonic organisms. The lowest DOM concentrations were measured in the groundwater samples and higher concentrations were measured in surface water and wastewater effluent. Similar trends were noted among the concentrations of DOM fractions with different MW; L-DOM, M-DOM, and H-DOM represent the DOM fractions with MW less than 600 Da, between 600 and 1000 Da, and over 1000 Da, respectively. It is worth noting that much of the DOM measured in SW2 is contained in the largest H-DOM size bin, and that SW2 actually had the lowest L-DOM concentration (0.33 mg L^{-1}) among the water samples. Finally, the sum of the three DOM concentrations measured for the three size bins is consistent with the DOM concentrations measured in the original water samples, demonstrating the robustness and reliability of the HPSEC method employed in this study.

Table 1
Water characterization results of six water samples.

Parameters	GW1	GW2	SW1	SW2	WW1	WW2
pH	8.2	8.3	8.2	8.1	8.3	8.2
[a]DOM	1.5	1.2	4.6	42.2	7.6	4.3
[b]L-DOM	0.4	0.4	0.6	0.3	1.4	1.0
[b]M-DOM	0.4	0.4	0.7	2.7	2.2	1.8
[c]LM-DOM	0.8	0.8	1.3	3.1	3.5	2.8
[b]H-DOM	0.4	0.4	3.6	54.6	3.5	1.4
[d]Sum-DOM	1.1	1.2	4.8	57.7	7.0	4.2
[e]Conductivity	272	343	334	432	780	616
[f]TDS	137	171	169	216	387	309
[g]F^-	0.1	0.0	0.0	0.0	0.0	0.0
Cl^-	8.9	11.2	53.6	33.4	174.5	115.2
NO_3^-	0.0	19.6	2.7	1.0	1.6	2.8
SO_4^{-2}	18.7	11.0	20.1	7.9	23.7	22.6
Li^+	0.0	0.0	0.0	0.0	0.0	0.0
Na^+	23.2	5.1	40.1	23.1	122.5	83.4
NH_4^+	0.0	0.0	0.0	0.0	15.9	0.2
K^+	1.2	0.8	2.8	2.5	9.2	5.1
Mg^{2+}	7.8	13.2	10.7	6.9	11.3	12.8
Ca^{2+}	26.8	47.2	24.8	21.3	16.5	32.6

[a]The DOM levels (mg L^{-1}) presented in this row are the overall DOC concentrations measured with unfractionated water samples; [b]The DOM levels (mg L^{-1}) presented in these rows are the DOC concentrations of low MW fraction, medium MW fraction, and high MW fraction, respectively; [c]The DOM levels (mg L^{-1}) presented in this row are the sum of L-DOM, M-DOM; [d]The DOM levels (mg L^{-1}) presented in this row are the sum of L-DOM, M-DOM, and H-DOM, which is another measurement of the overall DOM concentration in each water sample; [e, f]The TDS and conductivity of each water sample was measured with Fisher Accumet AP74 meter. The units of TDS and conductivity are ppm and μS, respectively; [g]The inorganic ions in each water sample were measured with Thermo DIONEX ICS-2100 Ion Chromatography system with the reference standards of all anions and cations reported in the above table used for the determination of retention time and quantification. The unit of each ion is mg L^{-1}.

3.2. Batch experiments

Of the 90 MPs employed in the batch experiments, eleven responded erratically to either the experimental (poor repeatability) or analytical conditions (poor limits of quantification). Therefore, we report data from the batch experiments for 79 of the 90 MPs. We first calculated the removal of each MP (R_{MP}) on each adsorbent in each water sample after 1 h of contact time as described in Equation (1). The data are provided in Tables S6 and S7 and the results are summarized in Fig. 1, which provides plots of R_{MP} on each adsorbent in each real water sample versus the R_{MP} on each adsorbent in nanopure water. Data for CCAC are provided in Fig. 1A for groundwater, Fig. 1C for surface water, and Fig. 1E for wastewater effluent. Analogous plots for CDP are provided in Fig. 1B, D, and 1F.

MP removal on CCAC was generally good after 1 h of contact time, but adsorption was inhibited in real water matrices relative to nanopure water; the degree to which R_{MP} was inhibited increased from groundwater to surface water to wastewater effluent. For example, whereas 75 (GW1) and 74 MPs (GW2) exhibited more than 50% removal in groundwater, only 11 (WW1) and 2 MPs (WW2) exhibited more than 50% removal in wastewater effluent. Among groups of MPs delineated by their charge, matrix

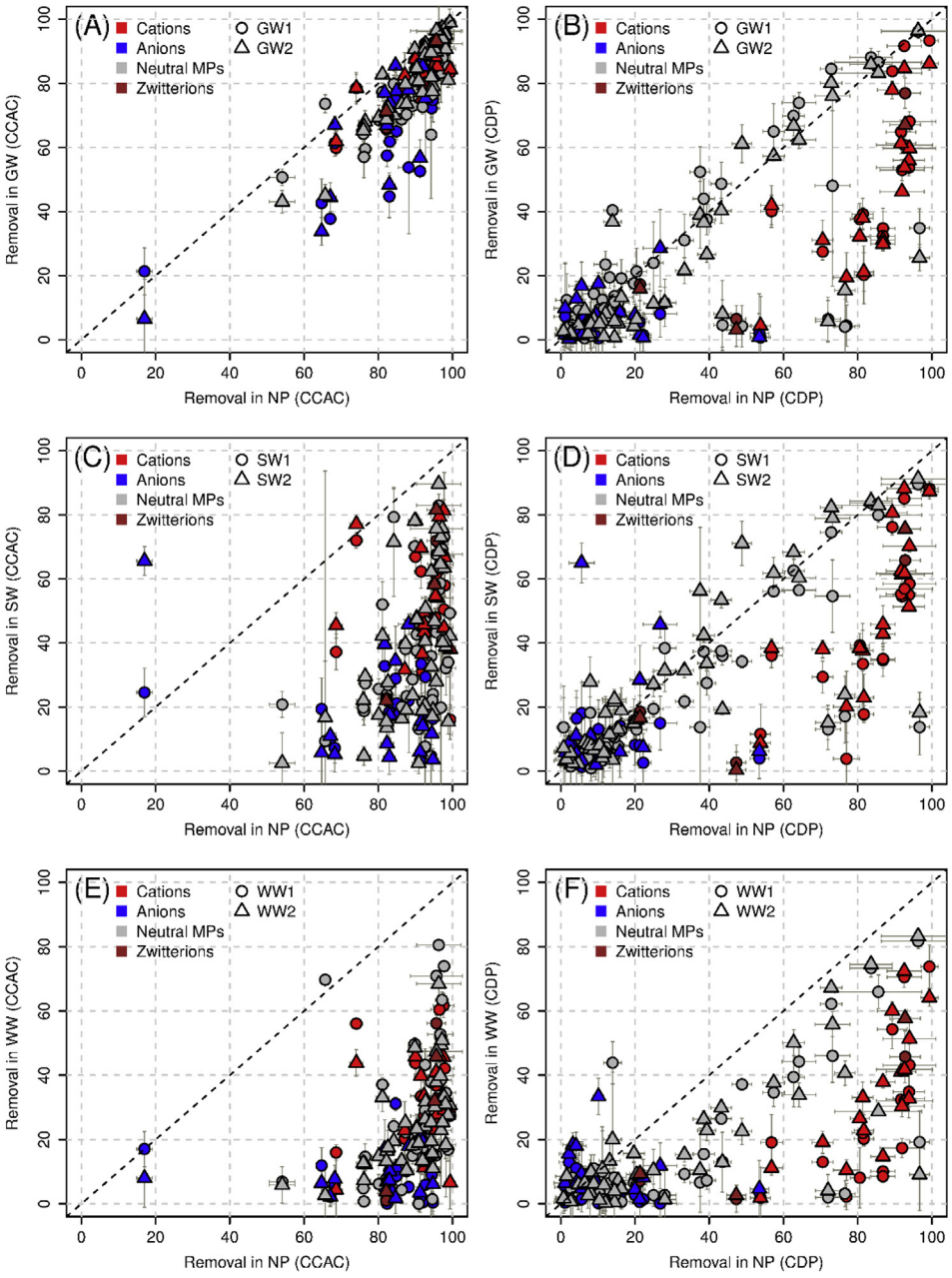

Fig. 1. Comparison of the removal of each MP: by CCAC in NP and GW (A), in NP and SW (C), in NP and WW (E); by CDP in NP and GW (B), in NP and SW (D), in NP and WW (F). Colors indicate the charge state of the MP at pH 7.4. Error bars represent the standard deviations of triplicate measurements. (For interpretation of the references to colour in this figure legend, the reader is referred to the Web version of this article.)

constituents had the largest effect on the R_{MP} of anionic MPs but effected MPs in other charge groups to varying extents regardless of their charge.

MP removal on CDP was more variable than on CCAC after 1 h of contact time, with 34 MPs exhibiting less than 20% removal in nanopure water, reflecting the greater selectivity of MP adsorption on CDP; the MPs that were removed to less than 20% in nanopure water were mostly anionic MPs or small and neutral MPs in agreement with our previous study (Ling et al., 2017). R_{MP} was inhibited to some extent for CDP in real water matrices relative to nanopure water, though the extent of adsorption inhibition was less than what was observed for CCAC. For example, of the 45 MPs that were removed to greater than 20% by CDP in nanopure water, 34 (in GW1) and 33 (in GW2), 30 (in SW1) and 40 (in SW2), and 21 (in WW1) and 28 (in WW2) were removed to greater than 20% in real water matrices. It is also clear from the data in Fig. 1 that the adsorption of cationic and zwitterionic MPs on CDP is selectively inhibited in the real water samples; the adsorption of neutral MPs is generally not inhibited in groundwater or surface water and is inhibited only to a limited extent in wastewater effluent whereas anionic MPs exhibit low affinity for CDP in all water matrices including nanopure water. To explore the selective adsorption inhibition of cationic MPs further, we calculated the fraction of the adsorption affinity (K_D values) that could be explained by electrostatic interactions by using the coefficients of a previously described QSAR model (Ling et al., 2019). We found a significant positive association (Permutation Test, $p < 0.01$) between the extent of adsorption inhibition for each cationic MP and the fraction

of its adsorption affinity attributed to electrostatic interactions. For example, the K_D values for cationic MPs morphine and albuterol on CDP are almost entirely explained by molecular descriptors that relate to electrostatic interactions; these two MPs exhibit the greatest adsorption inhibition in these experiments. In contrast, acebutolol and metoprolol are cationic MPs with K_D values that rely more on molecular descriptors related to hydrophobic interactions and these two MPs exhibit the least amount of adsorption inhibition in these experiments. Therefore, we attribute the selective inhibition of cationic MPs on CDP to a weakening of electrostatic interactions in real water matrices.

3.3. RSSCT experiments — breakthrough curves

We selected 15 MPs (5 cationic, 5 anionic, and 5 neutral) from among the 90 MPs studied in the batch experiments to evaluate MP removal and breakthrough in RSSCT experiments designed to simulate a PBF with an EBCT of 9.6 min. We performed the RSSCT experiments with all six real water samples for CDP@CMC and with GW1, SW1, and WW1 for CCAC. Breakthrough curves for all 15 MPs for all RSSCT experiments are provided in Figures S2 through S7 of the SD, and for representative anionic (naproxen), cationic (venlafaxine), and neutral (acetochlor) MPs in Fig. 2 (on an experimental time basis) and Fig. S8 (on a throughput (bed volumes) basis). Data for CCAC are provided in Fig. 2A, C, and 2E and data for CDP@CMC are provided in Fig. 2B, D, and 2F.

All three MPs exhibit gradual breakthrough on CCAC in GW1 and SW1 and relatively steep breakthrough in WW1, and the shapes of the breakthrough curves for each MP in each water matrix are similar. This observation corroborates previous findings that MP uptake on CCAC is relatively slow and non-selective (Ling et al., 2017). Specifically, each MP exhibits continuously increasing breakthrough in GW1 and SW1 until about 50% breakthrough is achieved after 120 h. Complete breakthrough is observed relatively quickly for each MP in WW1, with over 80% breakthrough observed in less than 20 h. The similar shapes of the breakthrough curves in GW1 and SW1 suggest similar adsorption kinetics and capacity of CCAC in these matrices, while the rapid breakthrough of each MP in the WW1 experiments demonstrate that the fouling caused by the WW1 matrix reduced the adsorption capacity of CCAC to a great extent. As demonstrated in a previous study, DOM with MW less than 1000 Da can inhibit MP adsorption on AC adsorbents to a much greater extent than DOM with MW greater than 1000 Da (Kennedy and Summers, 2015). Therefore, the rapid breakthrough can be attributed to the significantly elevated concentration of LM-DOM in WW1.

In contrast to the RSSCT experiments with CCAC, all MPs exhibited steep breakthrough in the RSSCT experiments conducted with CDP@CMC. Steep breakthrough curves in PBF processes are a general indication of rapid adsorption kinetics, which is a known feature of MP adsorption on CDP and CDP@CMC (Alzate-Sánchez et al., 2019; Ling et al., 2017). Importantly, these data demonstrate that rapid adsorption kinetics are preserved in column experiments and in the presence of matrix constituents. Rapid adsorption kinetics, coupled with the high adsorption capacity of CDP adsorbents, can be leveraged in PBF processes to increase the throughput of water treatment and the volume of water treated per day when the objective is to achieve low MP concentrations in the effluent. Further, rapid adsorption translates to narrow mass transfer zones within the PBF process, implying that only small fractions of unused adsorbent will be wasted when a process reaches its treatment capacity. The data in Fig. 2 also show that the breakthrough time for each of the three MPs is shorter in the wastewater effluent matrices than in the groundwater and surface water matrices, which could be attributed to the elevated concentration of L-DOM and the enhanced ionic strength in WW1 and

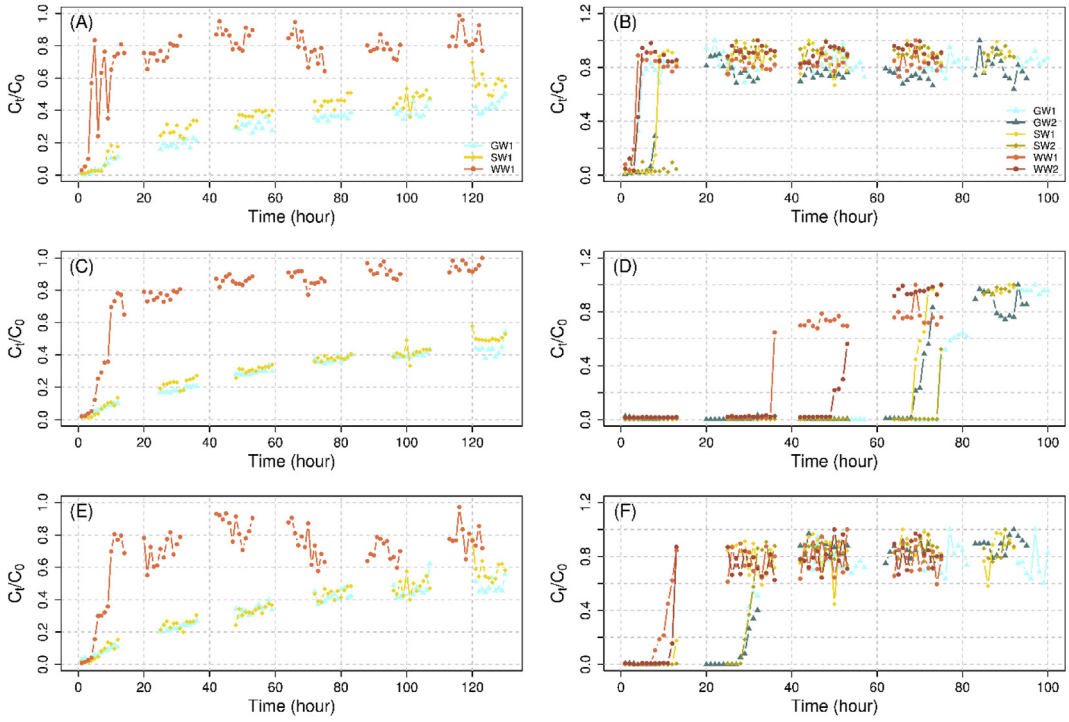

Fig. 2. Breakthrough curves of three example MPs with different charge states: (A) and (B) breakthrough curves of naproxen (the example of anions) on CCAC and CDP@CMC; (C) and (D) breakthrough curves of venlafaxine (the example of cations) on CCAC and CDP@CMC; (E) and (F) breakthrough curves of acetochlor (the example of neutral MPs) on CCAC and CDP@CMC. Missing data in breakthrough curves: all RSSCTs were run continuously for several days, during which no sample was collected from 12 p.m. to 7 a.m.

WW2 (see further discussion in the following). This effect is most pronounced for the cationic MP (Fig. 2D), in agreement with observations in batch experiments.

3.4. RSSCT experiments – treatment capacity

The operational capacity of a PBF process is typically evaluated based on the number of bed volumes treated before a certain level of contaminant breakthrough (Kennedy et al., 2015; Kennedy and Summers, 2015; Zietzschmann et al., 2016). In this study, we used the breakthrough curves to calculate the number of bed volumes treated before 10% contaminant breakthrough ($BV_{10\%}$) as has been done before in evaluating MP removal in RSSCT experiments (Kennedy and Summers, 2015; Zietzschmann et al., 2016). The $BV_{10\%}$ values of each MP on each adsorbent in each water sample is provided in Table S8 and are summarized in Fig. 3. Considering the different densities of CCAC (567 g/L) and CDP@CMC (433 g/L), the use rate of each adsorbent to achieve $BV_{10\%}$ for each MP in each water matrix is also provided in Table S9 to provide further insights into the relative adsorption capacity of CCAC and CDP@CMC in PBF processes.

The $BV_{10\%}$ values of all 15 MPs on CCAC were over 60,000 bed volumes in nanopure water (Table S8), but decreased substantially in real water matrices; the degree of $BV_{10\%}$ reduction increased from groundwater to surface water to wastewater effluent, in agreement with adsorption inhibition observations in batch experiments. Though 10 MPs exhibited $BV_{10\%}$ values of more than 5,000 bed volumes in GW1, no MP exhibited $BV_{10\%}$ values of more than 5,000 bed volumes in WW1. In addition, the $BV_{10\%}$ values of anionic MPs were inhibited to the greatest extent, whereas cationic and neutral MPs exhibited varying degrees of inhibition. These data are also consistent with our observations in batch experiments.

In contrast to the uniformly high $BV_{10\%}$ values of all MPs on CCAC in nanopure water, MP $BV_{10\%}$ values on CDP@CMC were more variable in nanopure water due to the selective adsorption on CDP (Table S8); all 5 cationic MPs exhibited $BV_{10\%}$ values over 60,000 bed volumes, which we attribute to the negative surface charge of CDP facilitating the adsorption of cationic MPs through electrostatic interactions (Klemes et al., 2018; Ling et al., 2019), whereas anionic and neutral MPs exhibited varying treatment capacity. Interestingly, three anionic MPs (diclofenac, gemfibrozil and naproxen) and one neutral MP (isoproturon), which were poorly removed by CDP in batch experiments, exhibit high $BV_{10\%}$ values over 55,000 bed volumes on CDP@CMC in nanopure water. This could be attributed to differences between the morphology of CDP and CDP@CMC and/or the distinct hydraulic conditions in batch and RSSCT experiments. The inhibition of MP adsorption capacity on CDP@CMC was also observed to some extent in real water matrices; of the 10 MPs that exhibited $BV_{10\%}$ values over 10,000 in nanopure, 7, 7, and 5 MPs exhibit $BV_{10\%}$ values over 10,000 in GW1, SW1, and WW1, respectively. Additionally, as observed in batch experiments, the $BV_{10\%}$ values of cationic MPs were inhibited to the greatest extent, whereas neutral and anionic MPs exhibited moderate to limited inhibition in real water matrices.

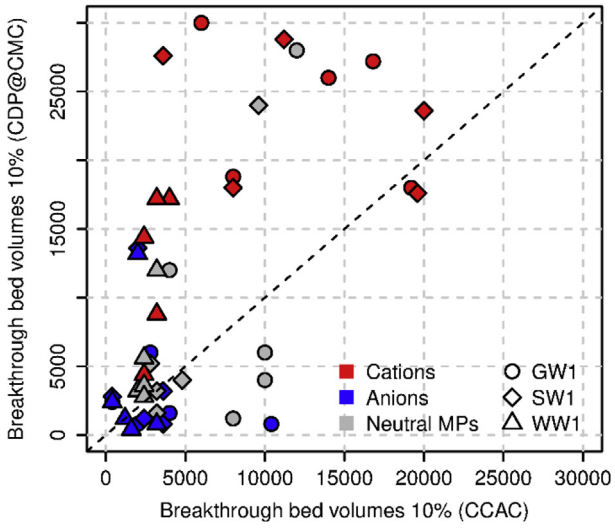

Fig. 3. Comparison of the 10% breakthrough bed volumes of 5 anionic MPs, 5 cationic MPs and 5 neutral MPs in GW1, SW1, and WW1 on CCAC and CDP. Colors indicate the charge state of the MP at pH 7.4. (For interpretation of the references to colour in this figure legend, the reader is referred to the Web version of this article.)

Though the MP removal on CDP@CMC was inhibited in real water matrices, the extent of inhibition was lower compared to that on CCAC. As shown in Fig. 3, for most MPs, the $BV_{10\%}$ values on CDP@CMC were much higher than that on CCAC with the exception of a few anionic and neutral MPs in GW1 which exhibited rather poor performance on both types of adsorbents. These data corroborate our observations in batch experiments that the extent of MP adsorption inhibition on CDP adsorbents is not as relevant to the complexity of the water matrix as that on CCAC, demonstrating less adsorption inhibition for CDP relative to CCAC. Further, the great treatment capacity of CDP@CMC is especially notable when we consider that there was nearly 25% less mass of CDP@CMC in the RSSCT experiments when compared to CCAC due to the differences in their densities; the data in Table S9 demonstrate that the use rate of each adsorbent to achieve $BV_{10\%}$ for each MP in each water matrix is frequently much lower for CDP@CMC compared to CCAC. Furthermore, approximately 77% of the mass of CDP@CMC is attributed to the cellulose microcrystals, which have been shown not to contribute to MP removal (Alzate-Sánchez et al., 2019).

3.5. Factors contributing to adsorbent fouling

The overall extent to which an adsorbent is fouled is generally determined by the composition of matrix constituents in real water matrices. To enable further insights on the fouling mechanisms of CCAC and CDP, we used the R_{MP} data and the $BV_{10\%}$ values to calculate the FSI for each adsorbent in each water sample, as described in Equations (2) and (3) for batch and RSSCT experiments, respectively. Because the inhibition of MP adsorption depended on the charge state of MPs, the FSI of each adsorbent was calculated both for all MPs and for MPs grouped by their charge states. The FSI of each adsorbent in each water sample for batch experiments are summarized in Fig. 4, and Tables S10 and S11 for batch and RSSCT experiments, respectively. To quantitatively interpret fouling mechanisms on both adsorbents, we investigated the associations between the FSIs calculated with MPs in different charge groups and all water quality parameters by means of Pearson correlations (Table S12).

As presented in Fig. 4A and Tables S10 and S11, the fouling of CCAC increases with the complexity of the water matrix (i.e., the fractions of DOM and the ionic strength). The general adsorption inhibition observed for all MPs could be attributed to direct site competition with L-DOM or M-DOM and/or pore blockage caused by H-DOM (Ding et al., 2008; Li et al., 2003; Newcombe et al., 1997). As seen in the Pearson correlation coefficients provided in Table S12, all groups of MPs exhibit the strongest positive correlations (>0.81, p-value <0.05) with the concentrations of LM-DOM (i.e., L-DOM plus M-DOM), indicating that direct site competition caused by LM-DOM could be a major contributor to the general adsorption inhibition observed for all MPs on CCAC. Further, MP

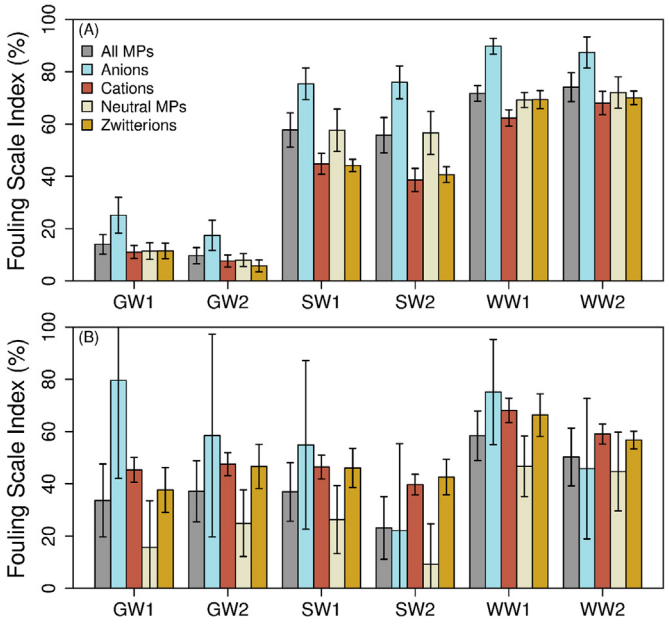

Fig. 4. The FSI of CCAC (A) and CDP (B) in each water matrix for batch experiments calculated with all 79 MPs, the subgroup of 17 cations, the subgroup 17 anions, the subgroup of 42 neutral MPs, and the subgroup of 3 zwitterionic MPs. Colors indicate the charge state of the MP subgroup on which the determination of the FSI was based. (For interpretation of the references to colour in this figure legend, the reader is referred to the Web version of this article.)

removal across all groups was only weakly correlated with H-DOM concentration (<0.27, p-value >0.50), indicating that pore blockage caused by H-DOM might not be a relevant fouling mechanism for CCAC. It is also worth noting that the anomalously high H-DOM concentration measured in SW2 did not result in a significant performance difference, further demonstrating that pore blockage caused by H-DOM might not be a relevant fouling mechanism for CCAC. These findings agree with observations in previous research that DOM with MW less than 1000 Da inhibits MP adsorption on AC adsorbents to a much greater extent than DOM with MW greater than 1000 Da (Kennedy and Summers, 2015; Zietzschmann et al., 2016).

The fouling of CCAC is greatest for anionic MPs (Fig. 4A, Tables S8 and S9). The selective adsorption inhibition observed for anionic MPs could be attributed to direct site competition with negatively charged L-DOM or M-DOM and/or to the presence of inorganic anions which screen the positive surface charge of CCAC (Newcombe, 1999; Summers and Roberts, 1988). As seen in the correlation coefficients provided in Table S12, the FSI calculated with the group of anionic MPs exhibit a strong positive correlation (0.85, p-value < 0.05) with the concentrations of LM-DOM, indicating that LM-DOM could be a major contributor to the selective adsorption inhibition of anionic MPs on CCAC. Further, the group of anionic MPs exhibit the weakest positive correlation with ionic strength when compared to the other groups of MPs. As a result, although the Pearson correlation coefficients alone cannot disentangle the effects of direct site competition and surface charge screening on the selective adsorption inhibition for anionic MPs, our data suggest that direct site competition with negatively charged LM-DOM might play an important role.

CDP and CDP@CMC notably exhibit nearly uniform FSIs across the water matrices (Fig. 4B, Tables S10 and S11). These data indicate greater fouling for CDPs relative to CCAC in the relatively clean groundwater matrices but less fouling for CDPs relative to CCAC in the more complex surface water and wastewater effluent matrices. The data also show significant adsorption inhibition for the group of anionic MPs, but that result must be interpreted with caution; the group of anionic MPs are not removed to great extents by CDP in nanopure water (Fig. 1) which inevitably led to great variability in the respective FSI, so the influence of matrix constituents on that adsorption cannot be reliably assessed. As observed in the data from the batch and RSSCT experiments and corroborated by the FSIs provided in Fig. 4B, the extent of fouling on CDPs is greatest for cationic and zwitterionic MPs. We have previously observed enhanced adsorption affinity for cationic MPs on CDPs (Ling et al., 2017), and hypothesize that the enhanced adsorption inhibition for the groups of cationic and zwitterionic MPs may result from the presence of inorganic cations that screen the negative surface charge of CDP. As presented in Table S12, the FSI calculated with the group of cationic MPs exhibits strong positive correlations with ionic strength for CDP (0.88, p-value < 0.05) and CDP@CMC (0.86, p-value < 0.05), indicating that ionic species could be major contributors to the enhanced adsorption inhibition of cationic and zwitterionic MPs on CDP adsorbents. However, we observed previously that NaCl does not result in significant adsorption inhibition (Ling et al., 2017), and the correlation coefficients in Table S12 do not allow us to identify specific inorganic ions that contribute the most to the observed adsorption inhibition. Finally, we observed the least amount of adsorption inhibition for the group of neutral MPs on CDP adsorbents. MP adsorption on CDP is associated with the formation of host-guest complexes in the interior cavity of the β-cyclodextrin monomers, which requires adsorbates to fit within a certain size range (Ling et al., 2019, 2017). Therefore, we expect that neutral MPs would compete only with neutral DOM species within a certain size range. The FSIs calculated with the group of neutral MPs exhibit strong positive correlations with the concentrations of L-DOM for CDP (0.94, p-value <0.05) and CDP@CMC (0.91, p-value <0.05), providing quantitative support to this proposed fouling mechanism. Additionally, the FSIs calculated with all groups of MPs exhibit weak or negative correlations with the concentrations of M-DOM and H-DOM, agreeing with our expectations that large molecules cannot bind to CDP due to size-exclusion (Ling et al., 2019, 2017; Szejtli, 1998). This result is particularly important because it corroborates the adsorption mechanism of CDP adsorbents demonstrated in our previous studies, validates our hypothesized fouling mechanism of CDP adsorbents, and explains the resilience of CDP adsorbents relative to CCAC in more complex water matrices.

4. Conclusions

- We measured the removal of 79 MPs on CCAC and CDP adsorbents in simulated BA-UF processes with water samples from six different sources. Overall, the extent of MP removal was greater and more consistent on CCAC than on CDP, which agrees with our previous study with TFN crosslinked CDPs.
- We observed increased adsorption inhibition for CCAC as the complexity of the water matrix increased, and enhanced adsorption inhibition was noted for anionic MPs. We observed lower extents of adsorption inhibition for CDP relative to CCAC, and selective adsorption inhibition for cationic MPs.
- We measured the breakthrough curves of 15 MPs on CCAC and CDP@CMC in RSSCT experiments that simulate PFB processes. Slow and constant breakthrough was observed for all MPs in columns packed with CCAC, though rapid and early breakthrough was observed for all MPs in experiments conducted with wastewater effluent. Rapid and late breakthrough was observed for all MPs in columns packed with CDP@CMC,

demonstrating fast adsorption kinetics and narrow mass transfer zones.

- Treatment capacity in RSSCT experiments was greater for CDP@CMC than CCAC for nearly all MPs in nearly all experiments; the exceptions are a few MPs that exhibited rather poor removal on both adsorbents.
- The general adsorption inhibition observed for CCAC was attributed to direct site competition with L-DOM and M-DOM. The selective inhibition of anionic MPs on CCAC was attributed to the abundance of negatively charged L-DOM and M-DOM. The resilience of CDP adsorbents to fouling in complex matrices was attributed to size-exclusion; only L-DOM directly competes with MPs for the active sites on CDP adsorbents. The selective adsorption inhibition of cationic MPs on CDP adsorbents was attributed to ionic strength.

Declaration of competing interest

The authors declare the following financial interests/personal relationships which may be considered as potential competing interests: Cornell University has filed US and international patent applications related to the porous cyclodextrin polymer studied in this manuscript. W.R.D. and D.E.H. serve on the scientific advisory board and have equity and/or stock purchase options in CycloPure, Inc., which is commercializing related porous cyclodextrin polymers and partially funded this study.

Acknowledgements

This work was supported by a grant from CycloPure, Inc., (D.E.H.) and the NSF Center for Sustainable Polymers, CHE-1901635 (W.R.D.).

Appendix A. Supplementary data

Supplementary data to this article can be found online at https://doi.org/10.1016/j.watres.2020.115551.

References

Alsbaiee, A., Smith, B.J., Xiao, L., Ling, Y., Helbling, D.E., Dichtel, W.R., 2015. Rapid removal of organic micropollutants from water by a porous β-cyclodextrin polymer. Nature 529, 190–194. https://doi.org/10.1038/nature16185.

Alzate-Sánchez, D.M., Ling, Y., Li, C., Frank, B.P., Bleher, R., Fairbrother, D.H., Helbling, D.E., Dichtel, W.R., 2019. β-Cyclodextrin polymers on microcrystalline cellulose as a granular media for organic micropollutant removal from water. ACS Appl. Mater. Interfaces 11, 8089–8096. https://doi.org/10.1021/acsami.8b22100.

Baird, R.B., Eaton, A.D., Rice, E.W., 2017. Standard Methods for the Examination of Water and Wastewater, 23rd ed. American Water Works Association (AWWA, WEF and APHA).

Benner, J., Helbling, D.E., Kohler, H.-P.E., Wittebol, J., Kaiser, E., Prasse, C., Ternes, T.A., Albers, C.N., Aamand, J., Horemans, B., Springael, D., Walravens, E., Boon, N., 2013. Is biological treatment a viable alternative for micropollutant removal in drinking water treatment processes? Water Res. 47, 5955–5976. https://doi.org/10.1016/j.watres.2013.07.015.

Bonvin, F., Jost, L., Randin, L., Bonvin, E., Kohn, T., 2015. Super-fine powdered activated carbon (SPAC) for efficient removal of micropollutants from wastewater treatment plant effluent. Water Res. 90, 90–99. https://doi.org/10.1016/j.watres.2015.12.001.

Bradley, P.M., Journey, C.A., Romanok, K.M., Barber, L.B., Buxton, H.T., Foreman, W.T., Furlong, E.T., Glassmeyer, S.T., Hladik, M.L., Iwanowicz, L.R., Jones, D.K., Kolpin, D.W., Kuivila, K.M., Loftin, K.A., Mills, M.A., Meyer, M.T., Orlando, J.L., Reilly, T.J., Smalling, K.L., Villeneuve, D.L., 2017. Expanded target-chemical analysis reveals extensive mixed-organic-contaminant exposure in U.S. Streams. Environ. Sci. Technol. 51, 4792–4802. https://doi.org/10.1021/acs.est.7b00012.

Carpenter, C.M.G., Helbling, D.E., 2018. Widespread micropollutant monitoring in the Hudson River Estuary reveals spatiotemporal micropollutant clusters and their sources. Environ. Sci. Technol. 52, 6187–6196. https://doi.org/10.1021/acs.est.8b00945.

Carpenter, C.M.G., Wong, L.Y.J., Johnson, C.A., Helbling, D.E., 2019. Fall creek monitoring station: highly resolved temporal sampling to prioritize the identification of nontarget micropollutants in a small stream. Environ. Sci. Technol. 53, 77–87. https://doi.org/10.1021/acs.est.8b05320.

Crittenden, J.C., Berrigan, J.K., Hand, D.W., 1986. Design of rapid small-scale adsorption tests for a constant diffusivity. Water Pollut. Control Fed 58, 312–319. https://doi.org/10.1016/S0262-1762(99)80122-9.

Crittenden, J.C., Reddy, P.S., Arora, H., Trynoski, J., Hand, D.W., Perram, D.L., Summers, R.S., 1991. Predicting GAC performance with rapid small-scale column tests. J. Am. Water Works Assoc. 83, 77–87.

de Ridder, D.J., Verliefde, A.R.D., Schoutteten, K., Van Der Linden, B., Heijman, S.G.J., Beurroies, I., Denoyel, R., Amy, G.L., Van Dijk, J.C., 2013. Relation between interfacial energy and adsorption of organic micropollutants onto activated carbon. Carbon N. Y. 53, 153–160. https://doi.org/10.1016/j.carbon.2012.10.042.

Ding, L., Snoeyink, V.L., Mariñas, B.J., Yue, Z., Economy, J., 2008. Effects of powdered activated carbon pore size distribution on the competitive adsorption of aqueous atrazine and natural organic matter. Environ. Sci. Technol. 42, 1227–1231. https://doi.org/10.1021/es0710555.

Kennedy, A.M., Reinert, A.M., Knappe, D.R.U., Ferrer, I., Summers, R.S., 2015. Full- and pilot-scale GAC adsorption of organic micropollutants. Water Res. 68C, 238–248. https://doi.org/10.1016/j.watres.2014.10.010.

Kennedy, A.M., Summers, R.S., 2015. Effect of DOM size on organic micropollutant adsorption by GAC. Environ. Sci. Technol. 49, 6617–6624. https://doi.org/10.1021/acs.est.5b00411.

Klemes, M.J., Ling, Y., Chiapasco, M., Alsbaiee, A., Helbling, D.E., Dichtel, W.R., 2018. Phenolation of cyclodextrin polymers controls their lead and organic micropollutant adsorption. Chem. Sci. 9, 8883–8889. https://doi.org/10.1039/C8SC03267J.

Knappe, D.R.U., Snoeyink, V.L., Roche, P., Prados, M.J., Bourbigot, M.M., 1997. The effect of preloading on rapid small-scale column test predictions of atrazine removal by GAC adsorbers. Water Res. 31, 2899–2909. https://doi.org/10.1016/S0043-1354(97)00148-6.

Kovalova, L., Knappe, D.R.U., Lehnberg, K., Kazner, C., Hollender, J., 2013. Removal of highly polar micropollutants from wastewater by powdered activated carbon. Environ. Sci. Pollut. Res. 20, 3607–3615. https://doi.org/10.1007/s11356-012-1432-9.

Li, C., Klemes, M.J., Dichtel, W.R., Helbling, D.E., 2018. Tetrafluoroterephthalonitrile-crosslinked β-cyclodextrin polymers for efficient extraction and recovery of organic micropollutants from water. J. Chromatogr. A 1541, 52–56. https://doi.org/10.1016/j.chroma.2018.02.012.

Li, Q., Snoeyink, V.L., Mariãas, B.J., Campos, C., 2003. Elucidating competitive adsorption mechanisms of atrazine and NOM using model compounds. Water Res. 37, 773–784. https://doi.org/10.1016/S0043-1354(02)00390-1.

Ling, Y., Klemes, M.J., Steinschneider, S., Dichtel, W.R., Helbling, D.E., 2019. QSARs to predict adsorption affinity of organic micropollutants for activated carbon and β-cyclodextrin polymer adsorbents. Water Res. 154, 217–226. https://doi.org/10.1016/j.watres.2019.02.012. https://search.crossref.org/?q=QSARs+to+predict+adsorption+affinity+of+organic+micropollutants+for+activated+carbon+and+%CE%B2-cyclodextrin+polymer+adsorbent.

Ling, Y., Klemes, M.J., Xiao, L., Alsbaiee, A., Dichtel, W.R., Helbling, D.E., 2017. Benchmarking micropollutant removal by activated carbon and porous β-cyclodextrin polymers under environmentally relevant scenarios. Environ. Sci. Technol. 51, 7590–7598. https://doi.org/10.1021/acs.est.7b00906.

Margot, J., Kienle, C., Magnet, A., Weil, M., Rossi, L., de Alencastro, L.F., Abegglen, C., Thonney, D., Chèvre, N., Schärer, M., Barry, D.A., 2013. Treatment of micropollutants in municipal wastewater: ozone or powdered activated carbon? Sci. Total Environ. 461–462, 480–498. https://doi.org/10.1016/j.scitotenv.2013.05.034.

Newcombe, G., 1999. Charge vs. porosity - some influences on the adsorption of natural organic matter (NOM) by activated carbon. Water Sci. Technol. 40, 191–198. https://doi.org/10.1016/S0273-1223(99)00656-3.

Newcombe, G., Drikas, M., 1997. Adsorption of NOM onto activated carbon: electrostatic and non-electrostatic effects. Carbon N. Y. 35, 1239–1250. https://doi.org/10.1016/S0008-6223(97)00078-X.

Newcombe, G., Drikas, M., Hayes, R., 1997. Influence of characterised natural organic material on activated carbon adsorption: II. Effect on pore volume distribution and adsorption of 2-methylisoborneol. Water Res. 31, 1065–1073. https://doi.org/10.1016/S0043-1354(96)00325-9.

Pochodylo, A.L., Helbling, D.E., 2017. Emerging investigators series: prioritization of suspect hits in a sensitive suspect screening workflow for comprehensive micropollutant characterization in environmental samples. Environ. Sci. Water Res. Technol. 3, 54–65. https://doi.org/10.1039/C6EW00248J.

Rossner, A., Snyder, S.A., Knappe, D.R.U., 2009. Removal of emerging contaminants of concern by alternative adsorbents. Water Res. 43, 3787–3796. https://doi.org/10.1016/j.watres.2009.06.009.

Schaefer, C.E., Nguyen, D., Ho, P., Im, J., Leblanc, A., 2019. Assessing rapid small-scale column tests for treatment of perfluoroalkyl acids by anion exchange resin. Ind. Eng. Chem. Res. 58, 9701–9706. https://doi.org/10.1021/acs.iecr.9b00858.

Schwarzenbach, R.P., Escher, B.I., Fenner, K., Hofstetter, T.B., Johnson, C.A., von Gunten, U., Wehrli, B., 2006. The challenge of micropollutants in aquatic systems. Science 313, 1072–1077. https://doi.org/10.1126/science.1127291 (80-.).

Sgroi, M., Anumol, T., Roccaro, P., Vagliasindi, F.G.A., Snyder, S.A., 2018. Modeling emerging contaminants breakthrough in packed bed adsorption columns by UV absorbance and fluorescing components of dissolved organic matter. Water Res. 145, 667–677. https://doi.org/10.1016/j.watres.2018.09.018.

Summers, R.S., Roberts, P.V., 1988. Activated carbon adsorption of humic substances.

II. Size exclusion and electrostatic interactions. J. Colloid Interface Sci. 122, 382–397. https://doi.org/10.1016/0021-9797(88)90373-6.
Szejtli, J., 1998. Introduction and general overview of cyclodextrin chemistry. Chem. Rev. 98, 1743–1753. https://doi.org/10.1021/CR970022C.
Thurman, E.M., Wershaw, R.L., Malcolm, R.L., Pinckney, D.J., 1982. Molecular size of aquatic humic substances. Org. Geochem. 4, 27–35. https://doi.org/10.1016/0146-6380(82)90005-5.
Wagoner, D.B., Christman, R.F., Cauchon, G., Paulson, R., 1997. Molar mass and size of suwannee river natural organic matter using multi-angle laser light scattering. Environ. Sci. Technol. 31, 937–941. https://doi.org/10.1021/es960594z.
Zietzschmann, F., Stützer, C., Jekel, M., 2016. Granular activated carbon adsorption of organic micro-pollutants in drinking water and treated wastewater – aligning breakthrough curves and capacities. Water Res. 92, 180–187. https://doi.org/10.1016/j.watres.2016.01.056.